JOURNAL OF CATALYSIS 45, 216–230 (1976)

Sulfur Dioxide Oxidation on Supported Molten V_2O_5–$K_2S_2O_7$ Catalyst

Influence of Liquid Diffusion Resistance

HANS LIVBJERG, KLAVS F. JENSEN, AND J. VILLADSEN

Instituttet for Kemiteknik, Technical University of Denmark, Lyngby, Denmark

Received March 9, 1976; revised July 26, 1976

The SO_2 oxidation activity of molten vanadium pentoxide–potassium pyrosulfate catalyst supported on porous SiO_2 particles has been studied. By proper selection of the experimental conditions the influence of diffusion of reaction components in the liquid phase can be measured. With low concentration of melt in the support the reaction is unhindered by diffusion and takes place as a homogeneous catalytic reaction in the liquid phase. Higher concentration of catalyst and large support pores yield poor liquid dispersion with the result that the activity is drastically reduced by liquid phase diffusion. From rate data and scanning electron microscopy it is shown that the liquid in the pore structure forms clusters, the dimensions of which vary with support pore size and catalyst concentration and may greatly exceed the support pore dimensions.

NOMENCLATURE

a, b, c	Parameters of Eq. (18)
c_{O_2}	Liquid phase oxygen concentration (moles cm^{-3})
$c_{O_2}^0$	c_{O_2} at gas/liquid interphase (moles cm^{-3})
$\mathfrak{D}_{O_2}$	Diffusivity of oxygen in liquid catalyst (cm^2 sec^{-1})
D_{SO_2}	Gas phase diffusivity in straight cylindrical pore (cm^2 sec^{-1})
$D_{SO_2,N_2}{}^G$	Binary gas diffusivity (cm^2 sec^{-1})
$D_{SO_2}{}^K$	Knudsen diffusivity (cm^2 sec^{-1})
h_{O_2}	Henry's law constant for gas/liquid phase equilibrium of oxygen (atm cm^3 mole^{-1})
k	Rate constant of Eq. 5
K_p	Gas phase chemical equilibrium constant for the reaction $SO_2 + \frac{1}{2}O_2 = SO_3$ (atm$^{-\frac{1}{2}}$)
$P_{SO_2}, P_{SO_3}, P_{O_2}$	Gas phase partial pressures (atm)
R_{SO_2}	Production rate per unit mass of support (moles sec^{-1} g^{-1})
(R_{O_2}')	Production rate per unit volume of liquid catalyst (moles sec^{-1} cm^{-3})
r_p	Pore radius of support (cm)
V_p	Pore volume of support per unit mass support (cm^3 g^{-1})
W_v	Vanadium content of impregnated catalyst as equivalent amount of V_2O_5 per unit mass support (g g^{-1})
α	Volume of liquid catalyst as fraction of support pore vol.
β	Kinetic parameter defined in Eq. (6)
δ	Equivalent slab thickness of liquid phase (cm)
Δ_{O_2}	"Effective diffusivity" of oxygen in liquid catalyst (moles atm^{-1} sec^{-1} cm^{-1})
ζ	Equilibrium oxygen partial pressure defined in Eq. (9) (atm)

η_l	Liquid phase effectiveness factor
θ_f	Porosity of liquid filled region
θ_p	Support porosity
ρ_v	Mass concentration of vanadium (as equivalent mass of V_2O_5) in liquid phase at reaction conditions (g cm^{-3})
ρ_s	Skeletal density of solid support phase (g cm^{-3})
κ	Liquid phase reaction rate constant defined in Eq. (9) (moles atm^{-1} sec^{-1} cm^{-3})
τ_f	Tortuosity factor for liquid phase diffusion
τ	Tortuosity factor for gas phase pore diffusion in catalyst pellets
Φ	Thiele modulus for liquid phase diffusion and chemical reaction.

INTRODUCTION

Liquid catalysts dispersed in an inert porous solid are utilized in many important syntheses. Notable examples of these so-called supported liquid phase (SLP) catalysts are the molten salt catalysts for vapor phase reactions that have recently been reviewed by Kenney (*1*), and include oxidation of sulfur dioxide, xylene or naphthalene by means of V_2O_5–$K_2S_2O_7$, and oxidation of hydrogen chloride or oxychlorination of organic compounds by promoted $CuCl_2$ catalyst. Other SLP-catalysts of immediate or potential importance are mentioned by Rony (*2*, *3*).

Investigation of the SO_2 catalyst has unequivocally shown that the oxidation takes place as a homogeneous reaction in the liquid phase, but due to liquid diffusion resistance only a thin surface layer is effective during reaction. In an SLP system the liquid phase may become sufficiently well dispersed and the effect of mass transport resistance in the liquid phase is greatly reduced. In principle it is possible to design an optimal SLP support pore structure by proper balancing of the mass transfer resistances in the liquid phase and in the residual pore system, i.e., the part of the support structure that is not filled with liquid. Theoretical work on this is reported by Rony (*2*, *3*) and by Livbjerg *et al.* (*8*).

The practical value of these design methods is at present quite limited. This is partly due to lack of experimental data for even the most fundamental properties of the liquid melt, for transport properties of the reactants and for kinetic parameters. Even worse is the lack of a proper model for the liquid distribution in the support. Often the formation of a uniform liquid layer covering the interior support surface is assumed, but its existence has never been verified experimentally and it is also thermodynamically unlikely to exist due to the high surface energy of the gas/liquid surface. Other liquid distribution models assume the liquid to fill pores up to a certain pore size or assume that liquid regions considerably larger then the pore dimensions are formed by coalescence of finer distributed liquid (*3*).

The problem is further complicated by the strong coupling that must exist between liquid distribution model, transport data for the liquid and intrinsic kinetics for the liquid phase reaction. For the best studied SLP reaction, namely oxidation of SO_2 on V_2O_5–$K_2S_2O_7$, the rate determining step, and even the composition of possible intermediates, are largely unknown in spite of more than 30 years of continued research.

The present investigation purports to interpret a set of carefully planned experiments with SO_2 oxidation catalyst by means of different liquid distribution models, assuming diffusion of oxygen in the liquid phase to be the important transport restriction and assuming the reaction rate to be first order in oxygen concentration. Even within its limited scope we believe that the experimental techniques and the models presented here can be used to study

other SLP systems, especially those with molten salt catalysts.

THEORY

Liquid Dispersion in Supported Liquid Phase Systems

Very little is known about the physical interaction between the catalyst melt and the support that disperses the liquid phase. Topsøe and Nielsen (*4*) showed that the melt in an SO_2 oxidation catalyst is mobile and tends to spread evenly through the pore structure in an initially nonuniformly impregnated particle. Kakinoki *et al.* (*14*) observed that the melt migrated from particle to particle in a mixture of impregnated and nonimpregnated particles during naphthalene oxidation. By porosimeter measurements on impregnated and activated SO_2 oxidation catalyst Tarasova *et al.* (*15*) found that the reduction in pore volume is much larger for the small pores in a given support than for the large ones especially for bidisperse pore structures where the macropore volume is almost unchanged. These observations give little insight in the actual dispersion of the liquid phase, but prove the liquid nature of the catalyst and also suggest that surface forces are active in determining the final degree of liquid dispersion.

We shall assume that the degree of liquid dispersion can be characterized by a single length parameter, δ, and this denotes the average maximum distance that the reactants must penetrate into the liquid from the gas/liquid surface in order to utilize the whole liquid volume for the chemical reaction. The support particles of the present investigation have pores with a narrow pore size distribution. In this way the complications of a broad or multidisperse pore size distribution are avoided and the interpretation of experimental results is somewhat simplified. For a uniform pore structure one would expect the degree of liquid dispersion (or δ) to be strongly influenced by the support pore radius r_p and by the fraction α of the pore volume which is filled with liquid. Some possible patterns of liquid distribution were discussed in (*8*). It is expedient to arrange such patterns in accordance with their degree of segregation of the liquid phase.

1. Uniform liquid film. Assuming long cylindrical pores and taking δ to be the equivalent slab thickness of the liquid phase (i.e., liquid volume divided by gas/liquid surface area) δ is obtained from

$$\delta = \frac{\frac{1}{2}r_p\alpha}{(1-\alpha)^{\frac{1}{2}}}. \qquad (1)$$

2. Dispersed liquid plugs. As discussed in (*8*) the surface forces tend to reduce the gas/liquid surface area by forming plugs in the pores so that the cross section of some pores is completely filled with liquid while other pores are empty. If the plugs are evenly distributed throughout the solid one can visualize the combined solid and liquid phases as one porous structure. This liquid-filled region is accessible from the gas phase anywhere along the interior surface of the residual pore system. Diffusion in the liquid-filled region is assumed to be equivalent to the liquid phase diffusion in a completely liquid-filled porous body. Hence δ can be estimated as the equivalent slab thickness of the liquid-filled region (i.e., the combined solid and liquid volumes divided by the residual pore surface area):

$$\delta = \frac{\frac{1}{2}r_p[(1/V_p\rho_s) + \alpha]}{(1-\alpha)}. \qquad (2)$$

3. Cluster models. The liquid can reduce gas/liquid surface area further by coalescence to clusters which form continuous liquid regions that are larger than the pore dimensions. Rony (*3*), by measurements of hydroformylation rate, produced evidence in support of cluster formation and this was incorporated in his model of liquid distribution. We have no knowledge of the

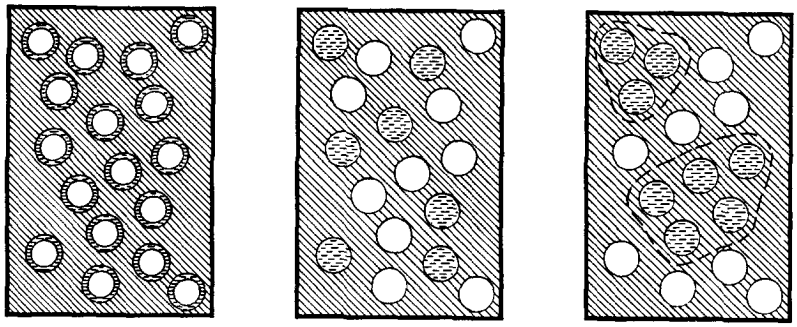

FIG. 1. Schematic representation of different types of liquid distribution in a porous solid. The hatched areas are the solid phase. Circles represent pore cross sections.

mechanisms leading to cluster formation or about the stability of cluster distributions. Hence a δ value for clusters can at present only be found from experiments.

In Fig. 1 the different types of liquid distribution are shown schematically.

Chemical Reaction and Transport Phenomena in SO_2 Catalyst

The overall reaction on industrial SO_2 oxidation catalyst involves many steps: these are diffusion of reactants in the porous support, absorption of reactants on to the liquid catalyst, diffusion and reaction in the liquid phase, desorption of SO_3 and diffusion of product back to the surface of the support pellet. Various intrinsic reaction mechanisms have been proposed (*1*, *9–11*). It is established that vanadium is present mainly as V^{5+} and V^{4+} compounds, probably combined with the pyrosulfate ion, and in proportions that vary with temperature and gas composition. Apart from this very little is known about the reaction scheme or the nature of intermediate liquid phase species.

The reaction is clearly diffusion restricted unless special care is taken to disperse the liquid phase. Holroyd and Kenney (*5*) estimated a penetration depth of 900 Å from oxygen absorption measurements with stirred pools of liquid catalyst. Polyakova *et al.* (*6*) measured the rate of SO_2 oxidation on catalyst film deposited on the surface of an inert nonporous material. They found that the oxidation rate at 485°C was proportional to liquid volume for films less than 2000 Å thick. With increasing film thickness the rate per volume catalyst decreases until the rate finally becomes proportional to the surface area of the melt. Somewhat different results were obtained with catalysts impregnated on porous supports (*7*), but the difficulties of estimating a realistic thickness of the dispersed liquid phase may presumably explain the discrepancies between these two investigations.

Solution of the chemical reaction-with-diffusion problem is much more difficult for a liquid phase catalytic reaction than for the ordinary pore diffusion problem in heterogeneous catalysis. Not only the reactants, but also the catalyst species and intermediates may have varying concentration through the liquid film and mass balances for all stoichiometrically independent reaction steps must be solved simultaneously.

With the present knowledge about the details of the SO_2 oxidation mechanism a simplified treatment is, however, entirely adequate. In our treatment of experimental data of this investigation we shall therefore

assume:

1. The catalyst composition is independent of film thickness except for the three dissolved overall reaction compounds.
2. SO_2 and SO_3 are much more soluble in the melt than O_2 which further reduces the number of independent mass balances.

The first assumption is supported by the two-step mechanism of Mars and Maessen (*9*)

$$SO_2 + 2V^{5+} + O^{2-} \rightleftarrows SO_3 + 2V^{4+} \quad (3)$$

$$\tfrac{1}{2}O_2 + V^{4+} \rightarrow V^{5+} + O^{2-}. \quad (4)$$

The individual rates of Eq. (3) are fast compared to the rate of Eq. (4) and thus the catalyst composition ($[V^{5+}]$, $[V^{4+}]$, $[O^{2-}]$) in the kinetic regime is established by the pseudo-equilibrium of Eq. (3) as a function of gas phase partial pressures of SO_2 and SO_3. Assumption (2) further ensures that catalyst composition does not change from the kinetic to the diffusion restricted regime. Boreskov *et al.* (*11*) have cast some doubt on Mars and Maessen's mechanism, but even so it is the best documented of many proposed mechanisms. For the present investigation where the emphasis is on a study of liquid dispersion models it gives a satisfactory picture of the intrinsic rate mechanism.

Assumption 2 concerning the relatively low O_2 solubility is supported by Holroyd and Kenney's (*5*) measurement of oxygen penetration in the melt.

Most empirical rate equations for SO_2 oxidation on V_2O_5–$K_2S_2O_7$ catalyst are approximately first order in oxygen partial pressure. Their general form is (*12*)

$$-R_{O_2}' = kP_{O_2}f(P_{SO_2}, P_{SO_3}, T)(1 - \beta^2), \quad (5)$$

with

$$\beta = \frac{1}{K_p}\frac{P_{SO_3}}{P_{SO_2}P_{O_2}^{\frac{1}{2}}}. \quad (6)$$

We propose to use Eq. (5) also for the intrinsic rate per volume liquid, i.e., we assume the rate determining step to be first order in oxygen concentration in the melt, where the oxygen concentration at the melt surface $c_{O_2}^0$ is given by Henry's law:

$$P_{O_2} = h_{O_2}c_{O_2}^0. \quad (7)$$

The intrinsic liquid phase kinetics are consequently assumed to be of the following form at an arbitrary position in the film:

$$-R_{O_2}' = kf(P_{SO_2}, P_{SO_3}, T) \times \left\{h_{O_2}c_{O_2} - \left(\frac{P_{SO_3}}{K_pP_{SO_2}}\right)^2\right\} \quad (8)$$

$$= \kappa(h_{O_2}c_{O_2} - \zeta), \quad (9)$$

where

$$\kappa = kf(P_{SO_2}, P_{SO_3}, T) \text{ and } \zeta = \left(\frac{P_{SO_3}}{K_pP_{SO_2}}\right)^2.$$

The temperature gradient through the liquid film is assumed to have negligible influence on the pseudo-first order rate constant κ and on the equilibrium parameter ζ. Both quantities are then independent of position in the film and they are given by P_{SO_2}, P_{SO_3}, and T in the gas phase just outside the liquid film.

Under these assumptions the overall reactant consumption in a uniform film of thickness δ can be expressed as:

$$-R_{SO_2} = -2R_{O_2} = 2V_p\alpha\eta_l\kappa(P_{O_2} - \zeta), \quad (10)$$

where V_p is the support pore volume, and α the fraction of pore volume filled with liquid. The liquid film effectiveness factor η_l is

$$\eta_l = \frac{\tanh\Phi}{\Phi}, \quad \Phi = \delta(\kappa/\Delta_{O_2})^{\frac{1}{2}}, \quad (11)$$

Δ_{O_2} is a "gas–liquid diffusion coefficient":

$$\Delta_{O_2} = \frac{\mathfrak{D}_{O_2}}{h_{O_2}}. \quad (12)$$

Thus the local rate in a catalyst particle with a uniform liquid film distribution is

obtained from Eqs. (1) and (10)–(12). For a region of the porous structure with liquid saturated pores an equivalent film thickness δ is defined by Eq. (11), with effective diffusivity (*8*):

$$\{\mathfrak{D}_{O_2}\}_{eff} = \frac{\theta_f \mathfrak{D}_{O_2}}{\tau_f}, \qquad (13)$$

τ_f is the tortuosity factor for the liquid filled porous material (Satterfield (*13*), Chap. 1), and θ_f the porosity of the liquid-filled region. The effectiveness factor η_l is again given by Eq. (11) and the "effective" gas–liquid diffusivity is now

$$\Delta_{O_2} = \frac{\mathfrak{D}_{O_2}}{h_{O_2}\tau_f}. \qquad (14)$$

With liquid distributions following the dispersed liquid plugs model or cluster models the local rate is obtained from Eqs. (10), (11) and (14) with δ from Eq. (2) for the dispersed plugs model.

EXPERIMENTAL METHODS

Catalysts were prepared by impregnating small particles of support material with an aqueous solution of AR-grade $VOSO_4$ and $KHSO_4$ (atomic ratio K/V = 3.5). Samples containing up to 8 g V_2O_5/100 g support are prepared by impregnating with solutions of varying reagent concentration. Surplus solution is removed by centrifugation followed by drying at 80°C. Higher catalyst concentration is obtained by 1–3 extra impregnations, drying at 80°C after each impregnation. To avoid loss due to resolution of already embedded catalyst from the support these secondary impregnations are made by titrating the solution to the particles until the pores are completely saturated with solution. The end-point is sharp as a change from "dry" to "sticky" behavior of the stirred particles is observed within one or two drops of solution. Before being used in rate measurements the catalyst is activated at 480°C by 6–12 hr exposure to 11% O_2, 7.5% SO_2 gas, preconverted to equilibrium.

The support is controlled-pore glass (CPG), a 96% SiO_2 product commercially available for chromatographic separation techniques from Electro-Nucleonics, Inc. (Fairfield, N. J.). This support material is ideal for the present purpose: it is chemically and thermally resistant up to 700°C, has a very narrow pore size distribution and a large pore volume. CPG is available with widely different mean pore diameters, e.g., from 3000–75 Å. After prolonged use in activity measurements the support can be regenerated by washing with dilute NH_3 and water. No change in pore volume to within 0.5% has ever been detected even after repeated impregnations and regenerations which confirms that the support is truly inactive to the catalyst and to the reaction components, and as a

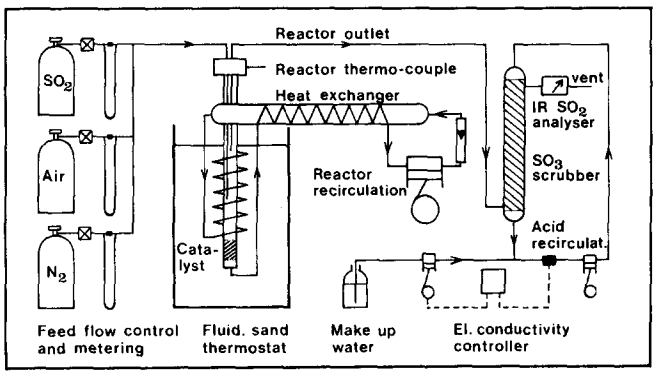

FIG. 2. Recirculation reactor.

corollary that it does not participate in the catalytic reaction mechanism.

By the use of small support particles it was ensured that gas phase pore diffusion did not influence the observed reaction rate.

Catalytic activity was measured in a recirculation reactor (see Fig. 2) with a high rate of recirculation to ensure isothermal operation with negligible gradients in the bulk gas phase.

The reactor is immersed in a fluidized sand bath in which temperature is controlled to within 0.2°C. Recirculation is provided by a twin head diaphragm compressor operating at 50°C to avoid condensation of SO_3. A countercurrent heat exchanger between reactor and compressor maintains the high temperature differential between reactor and compressor with the least possible disturbance of reactor temperature control. Both reactor and heat exchanger are of quartz glass connected with ground ball joints. Compressor material is stainless steel with PTFE/Viton diaphragms. Tubing material is stainless steel and PTFE with Viton O-rings. Use of an external displacement type recirculation device rather than internal recirculation is necessary because of the high pressure drop over the catalyst bed when using the small catalyst particles of the present investigation.

TABLE 1

Summary of Experimental Conditions

Support properties			
Pore radius (Å)	1530	243	63
Particle size (mesh)	20/30	80/120	80/120
Pore vol (cm^3/g)	1.02	0.97	0.92
Apparent bulk density (g/cm^3)	0.68	0.70	0.73
Porosity	0.69	0.68	0.67
Catalyst properties			
Potassium/vanadium = 3.5 atoms/atom			
Reaction conditions			
50% conversion of 11% O_2, 7.5% SO_2: P_{O_2} = 0.096, P_{SO_2} = 0.040, P_{SO_3} = 0.040 atm			
Total pressure, 1.04 atm			
Reactor diam, 18 mm			
Catalyst wt range, 0.12–3.0 g			
Feed flow range, 50–2000 st. cm^3/min			

Reactor feed is made up from metered streams of air, N_2 and SO_2 and total feed rate is manually adjusted to give a predetermined conversion of SO_2. Part of the reactor outlet stream passes through a countercurrent scrubber system in which SO_3 is quantitatively absorbed in 99% H_2SO_4, which is recirculated in a closed loop to keep it saturated with SO_2 and thus avoiding simultaneous absorption of SO_2. The SO_3-free gas is analyzed on-line for SO_2 in an infrared gas analyzer. The absorber acid concentration is kept constant by automatic addition of water (~1 ml/24 hr) in a conductivity control loop. The time constant of the absorber for SO_2 accumulation is ~5 min. This is of minor consequence since the time required to reach a new steady state after a change in reaction conditions is at least several hours for the catalyst. Calibration of the ir instrument is done by chemical SO_2 analysis as described in Ref. (*16*). Calculation of reaction rate also follows standard procedures described in, e.g., Refs. (*16, 17*).

RESULTS AND DISCUSSION

Support particles with pore size r_p = 63, 243, and 1530 Å were used. Catalytic activity was measured at 435, 480, and 530°C for different samples of catalyst with V_2O_5 content ranging from 0.65 to 26.6 g V_2O_5/100 g support. Catalyst properties and experimental conditions are summarized in Table 1.

The composition of the reactor feed was kept constant at 11% O_2, 7.5% SO_2 (balance N_2). The feed rate was adjusted to obtain approximately 50% SO_2 conversion. Minor variations from this standard condition were allowed, and the measured rate was extrapolated to the standard conditions using Mars and Maessen's rate expression (*9*). This was found to be a highly accurate procedure as shown by separate tests in which the experimental conditions were accurately adjusted to 50% conversion. The use of a standard gas

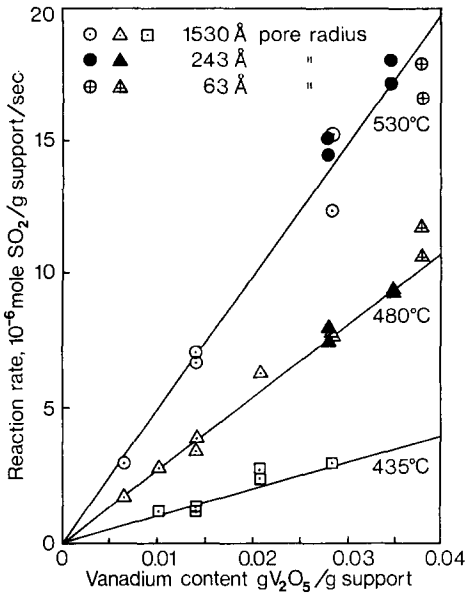

FIG. 3. Measured reaction rate for very dilutely impregnated catalysts with different support pore sizes. The rate is proportional to catalyst loading and independent of support pore size within experimental error.

composition for all measurements greatly simplifies the treatment of the data because the pseudo-first order rate constant κ of Eq. (9) then remains constant for constant temperature.

The normal duration of a run was 2–4 hr to ensure that the measured outlet conversion did not change any further. Every third or fourth run was extended to 15–18 hr and also measurements were frequently repeated after a full temperature cycle 435–530°C. Very stable results were obtained for samples with small V_2O_5 content (no liquid diffusion resistance) and mostly also for samples with very high V_2O_5 content. For samples with an intermediate V_2O_5 content the activity sometimes changed by 20–30% during the temperature cycles. The nature of this temperature effect is not clear. The activity variations seemed unsystematic and no permanent activity level was obtainable. Possibly redistribution or phase transformations of the liquid phase are responsible for these observations. The measured rate data are shown in Figs. 3–8.

Influence of Gas Phase Transport Resistance

The purpose of the present investigation is to study the properties of the liquid phase under experimental conditions where gas phase pore diffusion resistance is negligible. The following checks serve to assure that this assumption is valid.

Gas phase pore resistance is expressed through a gas phase effectiveness factor η_a. This is obtained from $(D_{SO_2})_{eff}$ and the observed rate, particle size, and gas composition assuming that the reaction rate is first order in SO_2 concentration and using the procedure described by Satterfield (*13*,

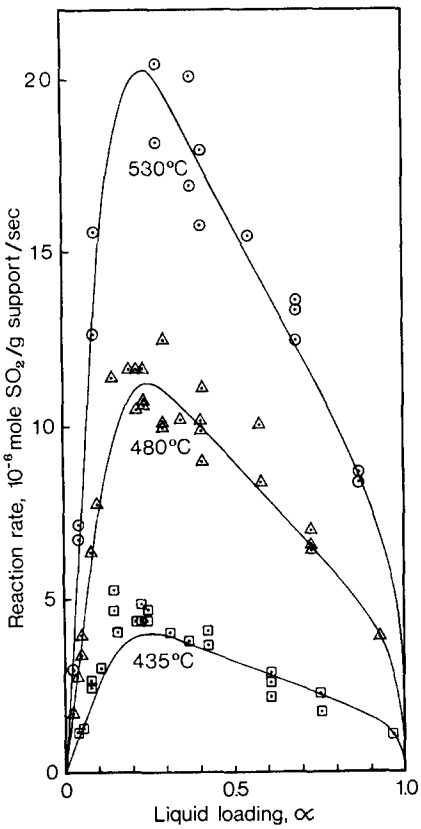

FIG. 4. Measured reaction rate, r_p = 1530 Å. The solid lines on Figs. 4–8 are computed regression curves based on Eq. (18) and the parameter values of Table 4.

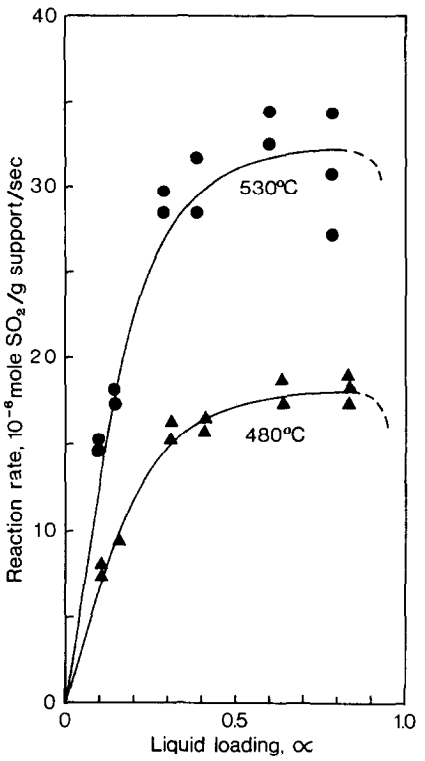

FIG. 5. Measured reaction rate, r_p = 243 Å.

Chap. 3.4). The effective pore diffusion coefficient is obtained from:

$$(D_{SO_2})_{eff} = \frac{\theta_p(1-\alpha)D_{SO_2}}{\tau} \qquad (15)$$

(Satterfield (*13*), Chap. 1) assuming that SO_2 mass transport through the catalyst particles occurs by gas phase pore diffusion only. $\theta_p(1-\alpha)$ is the residual porosity of the particles, and the tortuosity factor $\tau = 3$. D_{SO_2} is finally given by

$$D_{SO_2} = \left\{\frac{1}{D_{SO_2,N_2}{}^G} + \frac{1}{D_{SO_2}{}^K}\right\}^{-1},$$

where the Knudsen diffusion coefficient $D_{SO_2}{}^K$ is computed for a cylindrical pore with radius equal to the support pore radius. The computed η_a values were used to correct the measured rate data for gas phase pore diffusion. The corrections were always small and did not exceed 5% except for some of the measurements at the highest temperature, 530°C, for which η_a is shown as a function of pore size and fractional liquid loading in Fig. 9.

The influence of concentration and temperature gradients in the gas phase surrounding the catalyst particles is also negligible. The recirculation compressor yields a gas flow of ~1.5 Nm^3/hr and the recycle ratio, i.e., the fraction of gas recycled by the compressor, is between 0.96 and 0.997 for all runs. For the largest catalyst particles (20/30 mesh) the estimated heat and mass transfer coefficients are 0.01 cal/sec/cm^2/°C and 50 cm/sec (SO_2), respectively. Thus from Table 1 it can be ascertained that the temperature difference between bulk gas phase and particles never exceeds 0.5°C and that the corresponding composition change is also quite negligible. The maximum deviation between the measured temperature in the middle of the catalyst bed and that of the inlet or outlet is ~2°C assuming adiabatic conditions.

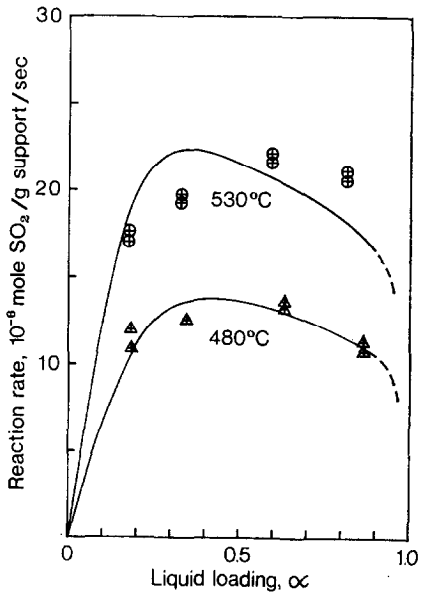

FIG. 6. Measured reaction rate, r_p = 63 Å.

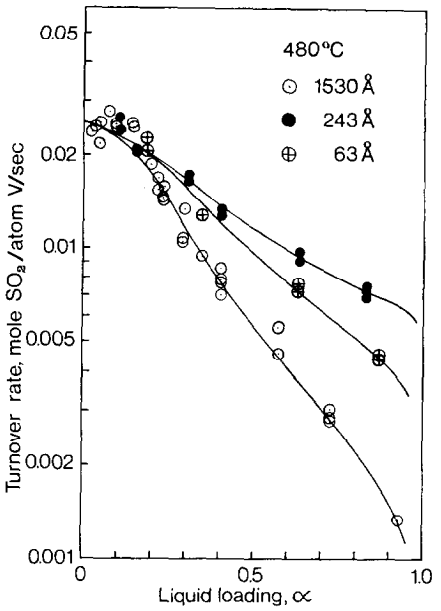

FIG. 7. Turnover rate (number of SO_2 molecules converted per vanadium atom in 1 sec) as a function of liquid loading and pore size at 480°C. In Figs. 7 and 8 the liquid effectiveness factor η_l is obtained as the ratio of the ordinate for a given α to the ordinate at $\alpha = 0$.

Interpretation of Rate Data

Figure 3 shows rate data for very small α. The rate is clearly independent of pore size and proportional to liquid loading in this α range. This result can be taken to prove that a homogeneous catalytic liquid phase reaction is being studied. For sufficiently small catalyst loading the liquid dispersion is perfect and all liquid is being utilized irrespective of the support pore structure. When the liquid loading is increased the rate per mole V_2O_5 drops drastically below the constant value obtained for small α. This is due to liquid phase diffusion resistance, and the rate becomes highly sensitive to changes in support pore size as seen in Figs. 7 and 8. It is noteworthy that the present results although qualitatively showing the same features for large α as the theoretical curves of (*8*) are obtained with no gas phase resistance and consequently they are attributable to liquid phase transport restrictions alone.

We shall now correlate the results with the liquid distribution models, Eq. (1), for a uniform film and Eq. (2) for dispersed plugs. The directly measured V_2O_5 content W_v g/g support is first transformed to fractional liquid loading α, the parameter that appears in the models:

$$\alpha = \frac{W_v}{\rho_v V_p}, \tag{16}$$

where ρ_v is the mass concentration of vanadium (as equivalent amount of V_2O_5) in the melt.

ρ_v could in principle be derived from the molar composition of the melt, but this is quite unsatisfactory since, e.g., the melt may absorb largely unknown amounts of gaseous reactants at different temperatures. Consequently ρ_v is determined simultaneously with the parameters κ and Δ_{O_2} [Eqs. (10), (12), (14)] by a weighted nonlinear least squares treatment of the rate data. The following functional is

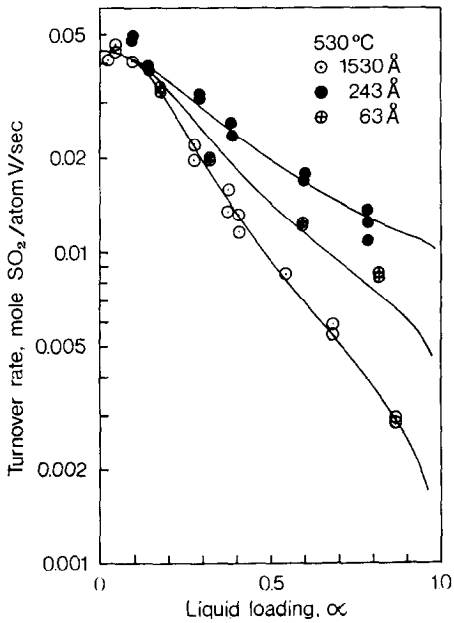

FIG. 8. Turnover rate as a function of liquid loading and pore size at 530°C.

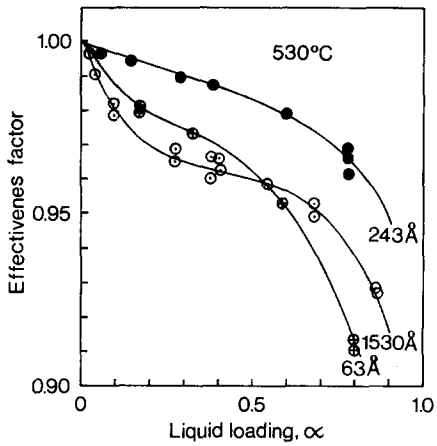

Fig. 9. Decrease of catalyst effectiveness due to gas phase pore diffusion at 530°C.

minimized:

$$sws = \sum \left(\frac{R_{SO_2,model} - R_{SO_2}}{R_{SO_2}} \right)^2, \quad (17)$$

where the weights $R_{SO_2}^{-1}$ are chosen since it is the relative error of R_{SO_2} rather than the absolute error of R_{SO_2} that is considered to be constant in all experiments.

Table 2 shows regression analysis results for the 480°C data using either the uniform liquid film—or the dispersed plug model. Due to a very severe liquid film transport resistance it was impossible to separate κ and Δ_{O_2} in the treatment of $r_p = 1530$ Å data with the dispersed plug model and consequently only their product is shown.

Δ_{O_2} is a physical property of the liquid phase which should be independent of support pore size. Obviously both models are very deficient as predictors of this quantity. The measurements of Polyakova *et al.* (*6*) for melts on a nonporous support were obtained at 485°C and the same catalyst composition as used here. From their data one can extract $\mathfrak{D}_{O_2}/h_{O_2} = 2 \times 10^{-13}$ mole atm^{-1} sec^{-1} cm^{-1} and by Eq. (12) this should be equal to the Δ_{O_2} value for the uniform film model. The corresponding value from Table 2 is $\sim 1.7 \times 10^{-16}$ mole atm^{-1} sec^{-1} cm^{-1} which is far too low. Correspondingly the entry 1.6×10^{-15} for the dispersed pore model would require a quite unrealistic liquid region tortuosity factor ($\tau_f \sim 10^3$) to be correct. As κ and Δ_{O_2} are strongly correlated through Eq. (11) the low Δ_{O_2} values must be due to gross underestimation of the δ value by either the uniform film or the dispersed plug models. Consequently a considerable coalescence of plugs to liquid regions with a much larger diffusion path δ than can be estimated from pore dimensions must take place.

From the slope of the straight lines in Fig. 3 κ can be computed using Eq. (10)

TABLE 2

Regression Analysis[a]

	Support pore radius (Å):	1530	243	63
Dispersed	κ (mole atm^{-1} sec^{-1} cm^{-3})		(3.2 ± 0.7) 10^{-4}	(4.0 ± 2.0) 10^{-4}
	$\kappa \cdot \Delta_{O_2}$ = (2.3 ± 0.2) 10^{-18}			
plug	Δ_{O_2} (mole atm^{-1} sec^{-1} cm^{-1})		(1.6 ± 1.0) 10^{-15}	(4.1 ± 3.6) 10^{-17}
model	ρ_v (g V_2O_5/cm^3 liquid)	0.30 ± 0.01	0.30	0.30
Uniform	κ (mole atm^{-1} sec^{-1} cm^{-3})	(4.3 ± 0.3) 10^{-4}	(3.2 ± 0.5) 10^{-4}	(3.4 ± 1) 10^{-4}
liquid film	Δ_{O_2} (mole atm^{-1} sec^{-1} cm^{-1})	(6.0 ± 0.8) 10^{-16}	(1.7 ± 0.8) 10^{-16}	(5.3 ± 2.7) 10^{-18}
model	ρ_v (g V_2O_5/cm^3 liquid)	0.282 ± 0.007	0.282	0.282
	No. of observations	36	13	7

[a] Estimation of κ, Δ_{O_2} and ρ_v from the rate data at 480°C using uniform liquid film model and dispersed plug model for the distribution of the liquid phase in the pores. 2σ confidence limits are shown with the computed parameters.

TABLE 3

Regression Analysis[a]

Temperature (°C):	435	480	530
κ (moles atm^{-1} sec^{-1} cm^{-3})	(1.6 ± 0.3) 10^{-4}	(4.3 ± 0.3) 10^{-4}	(7.9 ± 0.8) 10^{-4}
κ (from slope of Fig. 3)	(1.4 ± 0.3) 10^{-4}	(4.0 ± 0.5) 10^{-4}	(7.7 ± 0.8) 10^{-4}
ρ_v (g V_2O_5/cm^3 liquid)	0.27 ± 0.01	0.282 ± 0.007	0.30 ± 0.01

[a] Estimation of κ and ρ_v for support pore radius 1530 Å using the uniform liquid film model.

with $\eta_l = 1$ and Eq. (16). In Table 3 the results are compared with κ values obtained by the full regression analysis on all 1530 Å data and there is a very satisfactory agreement between κ results obtained by both methods as well as between the κ values in Table 2 for both liquid dispersion models and different support pore sizes.

The ρ_v values of Tables 2 and 3 are somewhat smaller than the estimate (0.34–0.38 g V_2O_5/cm^3 liquid) that can be obtained assuming the melt to be $V_2O_5 \cdot 3.5\ K_2S_2O_7$, but it is known from Tandy's measurements (*18*) that at lower temperatures SO_3 is being absorbed in excess of the pyrosulfate structure. Desorption of SO_3 at the high temperature can easily explain the variation of ρ_v with T as shown in Table 3. Consequently we have used ρ_v from Table 3 in the following calculations.

With the value of Polyakova *et al.* for $\mathfrak{D}_{O_2}/h_{O_2} = 2 \times 10^{-13}$ mole atm^{-1} sec^{-1} cm^{-1} at 485°C and (κ, ρ_v) from Table 3 the variation of apparent liquid diffusion path δ with α has been calculated by regression analysis based on the following expression:

$$\delta = a \frac{\alpha^b}{(1 - \alpha)^c}. \qquad (18)$$

The rate data at 480°C were analyzed using the cluster model, Eqs. (18) and (10), (11), and (14) with a liquid tortuosity factor $\tau_f = 2$.

Regression values for a, b, and c are shown in Table 4, and the experimentally determined δ-functions are compared with those of the dispersed plug model and the uniform film model in Fig. 10. It appears that δ is roughly proportional to α almost throughout the α-range and for all pore sizes. The small variation of δ with r_p for constant α is remarkable, by a factor of 2 only when r_p is varied from 1530 to 63 Å. For small r_p (243–63 Å) δ appears to be independent of r_p, which is a strong indication that clusters of liquid are formed independently of pore radius. Even at the largest pore size $\delta_{\alpha=0.5}$ is 5–6 times larger than the pore dimension.

With the experimentally determined δ-function [Eq. (18)], which is assumed to be the same for all temperatures, the rate data for T = 435 and 530°C are used to compute the temperature dependence of $\mathfrak{D}_{O_2}/h_{O_2}$. The results are shown in Table 5. $\mathfrak{D}_{O_2}/h_{O_2}$ appears to increase with temperature in a reasonable way. The last column of Table 5 reflects the variation of the Thiele modulus Eq. (11) with temperature: both κ and $\mathfrak{D}_{O_2}/h_{O_2}$ increase approximately in the same way with T both with an apparent activation energy of roughly 20 kcal.

TABLE 4

Determination of the Parameters of the δ-Function[a]

Support pore radius	a (Å)	b	c	$\delta(\alpha = \frac{1}{2})$ (Å)
1,530	12,700	1.25	0.35	6,800
243	6,400	0.96	~0	3,300
63	7,800	1.1	0.13	4,000

[a] Eq. (18).

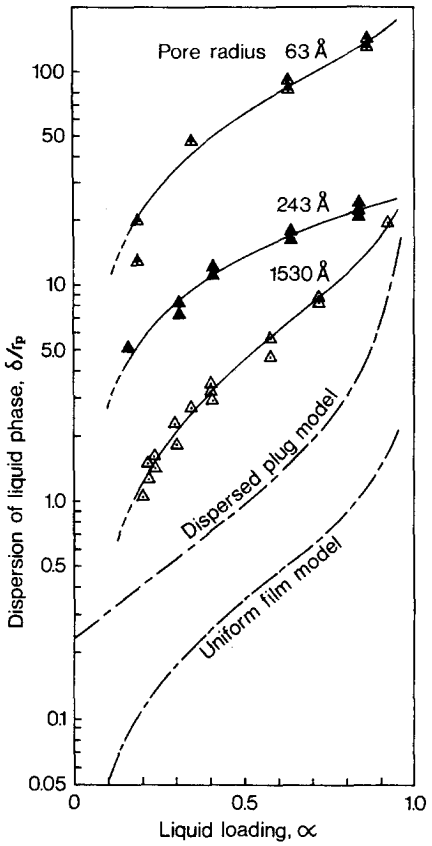

FIG. 10. Degree of liquid dispersion (as δ/r_p) computed from the rate data and compared with the simple distribution models (1) and (2).

Therefore the Thiele modulus is almost independent of T. Hence the degree of rate reduction caused by the liquid phase transport is hardly temperature dependent in the range 435–530°C.

TABLE 5

Temperature Variation of $\mathfrak{D}_{O_2}/h_{O_2}$[a]

Temperature (°C)	Support pore radius (Å)	$\mathfrak{D}_{O_2}/h_{O_2}$ (mole atm^{-1} sec^{-1} cm^{-1})	$\kappa h_{O_2}/\mathfrak{D}_{O_2}$ (cm^{-2})
435	1530	$(0.72 \pm 0.07)\ 10^{-13}$	1.9×10^9
480		2×10^{-13}	2.0×10^9
530	1530	$(3.3 \pm 0.15)\ 10^{-13}$	2.3×10^9
	243	$(3.3 \pm 0.2)\ 10^{-13}$	2.3×10^9
	63	$(2.6 \pm 0.3)\ 10^{-13}$	3.0×10^9

[a] The value at 480°C is from Ref. (6).

Direct Observation of Catalyst by Scanning Electron Microscopy (SEM)

On solidification the catalyst melt forms an amorphous phase, and there is no reason to believe that the catalyst dispersion is seriously altered by this process. Hence a study at room temperature of cooled catalyst samples may give an independent and more direct characterization of the catalyst distribution. The largest pore size (1530 Å) samples could be observed by SEM (JEOL JSM-Y3 microscope) and results are shown in Figs. 11 and 12 for the samples used in the rate measurements.

The very regular appearance of CPG pore structure is clearly observed in the picture (Fig. 11) of an unimpregnated sample and it is quite evident that the catalyst is arranged in clusters much larger than the pore dimensions (Fig. 12).

CONCLUSIONS

Two observations are of direct interest for the SO_2 oxidation system with a supported V_2O_5–$K_2S_2O_7$ melt.

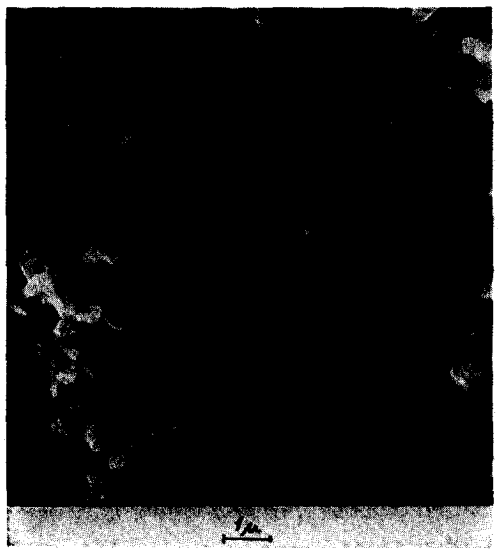

FIG. 11. SEM microphotograph (secondary electron image) of unimpregnated CPG support. (r_p = 1530 Å).

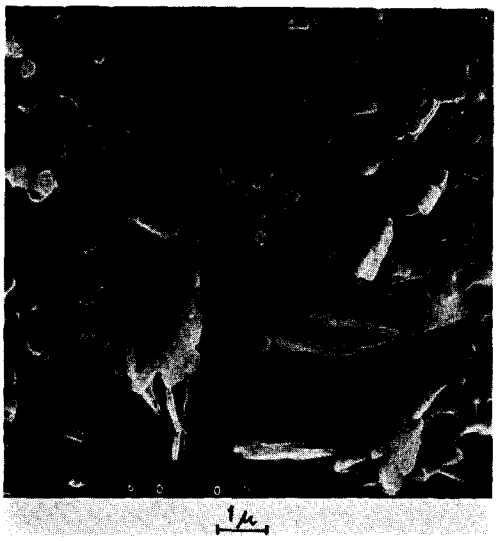

FIG. 12. SEM microphotograph of a fracture surface in an impregnated and used CPG catalyst particle (r_p = 1530 Å). Catalyst material clusters are observed as continuous regions without pore voids with dimensions of several pore diameters.

First, for dilutely impregnated catalysts the reaction rate is independent of support pore size and proportional to fractional liquid loading α. This confirms that SO_2 oxidation is a homogeneous catalytic reaction in the liquid phase.

Secondly, if the liquid phase is poorly dispersed resistance to diffusion in the melt will drastically reduce the catalytic activity. Poor dispersion is favored by large support pores and high fractional liquid loading.

Therefore, distribution of the liquid phase in the support pores and physical properties of the liquid phase such as solubility and diffusivity of reaction components are important parameters in an optimal catalyst formulation for supported liquid phase catalysts.

The liquid dispersion can roughly be described by the average length (δ) that reactants must diffuse from gas/liquid boundary into the liquid phase to utilize the whole catalyst volume for reaction. At present no reliable theory exists for the prediction of δ. The rate data of the present investigation show that the melt tends to form clusters in the monodisperse SiO_2 pore structure used as support, and this result is confirmed by scanning electron microscopy on cooled samples. The size of the clusters depends on fractional liquid loading and in a remarkably irregular way on support pore radius. The cluster size can greatly exceed the pore dimensions. These observations prove that simple liquid distribution models such as, e.g., the uniform film model are not generally applicable as predictors of δ and can lead to very erroneous results.

The simplified model of Eqs. (10)–(14) which is used to describe diffusion and chemical reaction in the liquid phase is based on the theory of Mars and Maessen Eqs. (3)–(4).

If the kinetic phenomena in the melt cannot be described by single reaction kinetics more refined models must be used to account quantitatively for the liquid phase diffusion kinetics since liquid phase transport restriction may lead to drastic overall composition changes in the catalyst when passing from the kinetic-controlled to the diffusion-controlled regime. Experimental evidence that such phenomena are important for the SO_2 oxidation catalyst in the low temperature range <435°C will be described in an ensuing paper.

ACKNOWLEDGMENT

We are indebted to Inge Hansson and Flemming Kragh for the electron microphotos. These photos were taken by the Electron Microscope Group at the Technical University of Denmark.

REFERENCES

1. Kenney, C. N., *Catal. Rev. Sci. Eng.* **11**, 197 (1975).
2. Rony, P. R., *Chem. Eng. Sci.* **23**, 1021 (1968).
3. Rony, P. R., *J. Catal.* **14**, 142 (1969).
4. Topsøe, H., and Nielsen, A., *Trans. Dan. Acad. Tech. Sci.* **1**, 1 (1948).
5. Holroyd, F. P. B., and Kenney, C. N., *Chem. Eng. Sci.* **26**, 1971 (1971).

6. Polyakova, G. M., Boreskov, G. K., Ivanov, A. A., Davydova, L. P., and Marochkina, G. A., *Kinet. Katal. (USSR)* **12**, 666 (1971). (Eng. transl. p. 586).

7. Boreskov, G. K., Dzis'ko, V. A., Tarasova, D. V., and Balaganskaya, G. P., *Kinet. Katal. (USSR)* 11, 181 (1970). (Eng. transl. p. 144).

8. Livbjerg, H., Sørensen, B., and Villadsen, J., *Advan. Chem. Ser.* **133**, 242 (1974).

9. Mars, P., and Maessen, J. G. H., *Proc. Int. Congr. Catal., 3rd*, 1, 226 (1964).

10. Mars, P., and Maessen, J. G. H., *J. Catal.* **10**, 1 (1968).

11. Boreskov, G. K., Polyakova, G. M., Ivanov, A. A., and Masdikhin, V. M., *Dokl. Akad. Nauk. USSR* **210**, 626 (1973). (Eng. transl. p. 423).

12. Livbjerg, H., and Villadsen, J., *Chem. Eng. Sci.* **27**, 21 (1972).

13. Satterfield, C. N., "Mass Transfer in Heterogeneous Catalysis." M.I.T. Press, Cambridge, Mass., 1970.

14. Kakinoki, H., Sahara, N., Kamata, I., and Aigami, Y., *Shokubai* **4**, 113 (1962).

15. Tarasova, D. V., Boreskov, G. K., and Dzis'ko, V. V., *Kinet. Katal. (USSR)* **9**, 1111 (1968).

16. Livbjerg, H., and Villadsen, J., *Chem. Eng. Sci.* **26**, 1495 (1971).

17. Pirjamali, M., Livbjerg, H., and Villadsen, J., *Chem. Eng. Sci.* **28**, 328 (1973).

18. Tandy, G. H., *J. Appl. Chem.* **6**, 68 (1956).